3.2 CHARACTERIZATION OF PRECIPITATES IN CUBIC SILICON CARBIDE IMPLANTED WITH $^{25}Mg^{+}$ IONS—W. Jiang, S. R. Spurgeon, J. Liu, D. J. Edwards, D. K. Schreiber, C. H. Henager, Jr., R. J. Kurtz (Pacific Northwest National Laboratory), and Y. Wang (Los Alamos National Laboratory)

OBJECTIVE

The aim of this study is to characterize precipitates in Mg^{+} ion implanted and high-temperature annealed cubic silicon carbide using scanning transmission electron microscopy, electron energy loss spectroscopy and atom probe tomography.

SUMMARY

This progress report presents results from high-resolution scanning transmission electron microscopy (STEM), electron energy loss spectroscopy (EELS) and atom probe tomography (APT). The APT study has been performed for cubic silicon carbide (3C-SiC) implanted to 9.6×10^{16} $^{25}Mg^{+}/cm^{2}$ at 673 K and subsequently annealed at 1073 and 1573 K for 2, 6, and 12 h in an Ar environment. The ^{25}Mg isotope was chosen to differentiate it from $^{12}C_2$ clusters in APT. STEM and EELS characterizations have been carried out for the same 3C-SiC sample annealed at 1573 K for 12 h. The APT results show a faster Mg clustering process during isochronal annealing (12 h) at a higher temperature while growth to larger Mg clusters on the average occurs during isothermal annealing (1573 K) for a longer time. The STEM-EELS study suggests that some of the precipitates have a core (MgC_2)-shell (Mg_2Si) microstructure. The precipitate size and number density are determined to be 2-8 nm and ~10^{18} $/cm^{3}$, respectively.

PROGRESS AND STATUS

Introduction

Calculations by Sawan, *et al*. [1] have predicted significant production of transmutants in silicon carbide under high-energy neutron irradiation in a fusion environment. At 100 dpa, there are ~0.5 at.% Mg, 0.2 at.% Be and 0.15 at.% Al generated in SiC in addition to 2.2 at.% He and 0.84 at.% H. The impact on the structural stability and thermomechanical properties due to the presence of the impurities, gas species and irradiation-induced defects in SiC is currently unknown, but could potentially limit the material's service lifetime. We have initiated an experimental study to investigate the structural effects of Mg in 3C-SiC by performing a series of ion implantation experiments. Our previous study [2] suggests that precipitates of cubic Mg_2Si and tetragonal MgC_2 are likely formed in 3C-SiC implanted to 9.6×10^{16} $^{24}Mg^{+}/cm^{2}$ at 673 K and subsequently annealed at 1573 K for 12 h in Ar environment. Evidence for the formation of these precipitates was obtained from a fast Fourier transformation (FFT) of an atomic-level resolution high-angle annular dark field (HAADF) STEM micrograph [2]. This study focuses on confirmation and characterization of these possible precipitates in $^{25}Mg^{+}$ ion implanted 3C-SiC using STEM, EELS mapping and APT. Some of the recent data are presented here. More results and discussion will be reported in a full-length manuscript to be prepared for journal publication.

Experimental Procedure

As described in our previous semiannual reports [3,4], 3C-SiC was implanted 7° off the surface normal with 200 keV $^{25}Mg^{+}$ ions at 673 K to an ion fluence of 9.6×10^{16} ions/cm^{2}, corresponding to ~6 at.% Mg and ~53 dpa at their respective peak maxima based on SRIM simulations [5]. Utilization of $^{25}Mg^{+}$ ions is needed to differentiate it from $^{12}C_2$ clusters in APT using time-of-flight mass spectrometry. The implanted samples were cleaved into smaller pieces for thermal annealing under various conditions. Isothermal annealing at 1573 K was performed for 2, 6 and 12 h in an Ar environment, while isochronal annealing for 12 h was done at 1073 and 1573 K. Using a focused ion beam (FIB) secondary electron microscope (FEI Helios NanoLab), one STEM specimen was prepared for 3C-SiC implanted with ^{25}Mg ions and annealed at 1573 K for 12 h. STEM was performed using a Cs-corrected JEOL ARM 200CF TEM-STEM. Equipped

with a cold field emitter, the microscope is capable of sub-Å spatial resolution under HAADF STEM imaging. The high-brightness source allows for a fast acquisition of EELS utilizing the latest Gatan Quantum 965 spectrometer. STEM and EELS were performed at both 200 and 80 kV, with the latter being used to minimize sample damage. APT examinations for a total of 5 implanted specimens prior to annealing and under the above-mentioned annealing conditions were carried out at a temperature of 44 K and a bias voltage ranging from 5.5 to 8.5 kV with a laser power of 60 – 80 pJ/pulse at a frequency of 125 kHz. The detection efficiency was 36% with an average detection rate of 0.4%. The total ions collected for each needle range from 3 to 5 M ions. The same specimen of $^{25}Mg^{+}$ ion implanted 3C-SiC annealed at 1573 K for 12 h was selected for study by STEM-EELS and APT for a direct comparison of results.

Results and Discussion

The microstructure in 3C-SiC implanted to 9.6×10^{16} $^{25}Mg/cm^2$ at 673 K and annealed at 1573 K for 12 h in Ar has been examined by HAADF STEM and a typical micrograph near the damage peak is shown in Figure 1 for a general view of features along zone axis [011]. A distribution of unidirectionally aligned tetrahedra is observed with two sides of the triangular shape parallel to [1-11] and [11-1], and the other parallel to [01-1], as indicated in the figure. The size of the tetrahedra ranges from 2 to 8 nm. This microstructure confirms our previous observation [2] of 3C-SiC implanted with ^{24}Mg and annealed under the same conditions. Kondo, *et al*. [6] have reported similarly aligned tetrahedra in 3C-SiC irradiated with neutrons at 1733 K. Their report indicates that the tetrahedra in 3C-SiC are voids based on under- and over-focus imaging and the different surface energies between Si- and C-terminated polar surfaces. This is in a contrast to stacking fault tetrahedra (SFTs) that are observed in high-temperature irradiated face-centered cubic metals and alloys [7]. Faceted voids have also been observed [8] in 3C-SiC irradiated with Ag ions at room temperature and subsequently annealed at 1873 K. The material was completely amorphized after the ion irradiation and a recrystallization process occurred during a subsequent thermal annealing. In this study, irradiation was performed at 673 K, which is above the critical temperature (~550 K) for amorphization of SiC. At this temperature, self-interstitials and implanted Mg in SiC migrate and cluster to some extent, but vacancies are not mobile, leaving behind excess vacancies in the as-implanted 3C-SiC. It is also expected that the vacancy concentration is much higher than the Mg concentration (6 at.%) in this region (~53 dpa). Subsequent annealing at 1573 K could lead to formation of vacancy clusters and voids. However, this process could be mediated by Mg atoms that should precipitate at the same time and can involve Si and C atoms in the process. A full understanding of this complex process requires a computational study. We also notice that the tetrahedra in Figure 1 show different contrasts, which are related to Mg concentrations, as will be discussed below. The specimen thickness in this region was determined by EELS to be ~30 nm. The number density of the tetrahedra is estimated to be ~10^{18} cm^{-3}.

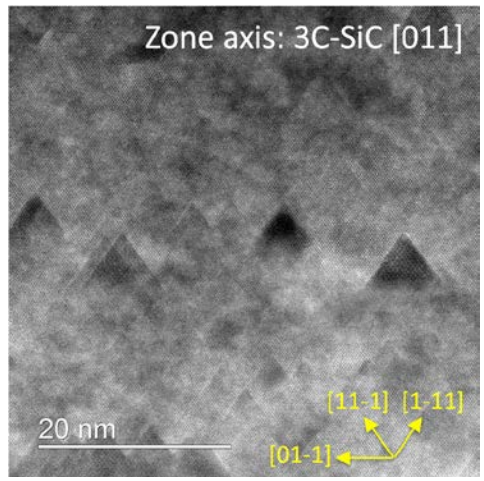

Figure 1. HAADF micrograph taken near the middle of the damage band of 3C-SiC implanted to 9.6×10^{16} $^{25}Mg/cm^2$ at 673 K and annealed at 1573 K for 12 h in Ar. Unidirectionally aligned tetrahedra appear with a number density of 1×10^{18} cm^{-3}.

A high-resolution HAADF STEM micrograph near the damage peak is shown in Figure 2. The dark tetrahedron of ~8 nm in size in the center appears to exhibit a different lattice with a coherent interface with the 3C-SiC matrix. Dislocations or stacking faults inside or outside the tetrahedron are not observed. There is an overlap of tetrahedra due to specimen thickness. The corresponding power spectrum from the micrograph is shown in Figure 2(b), which is consistent with our previous observations [2]. Three groups of different patterns are identified for 3C-SiC, cubic Mg_2Si and tetragonal MgC_2, as shown by

white, blue and red arrows in the figure, respectively. The orientation relationships are $Mg_2Si(110)//3C\text{-}SiC(110)$ and $MgC_2(110)//3C\text{-}SiC(110)$ with lattice mismatch of ~1% in both cases. It should be noted that as Mg_2Si and MgC_2 decompose at 873 and 1073 K, respectively, the possible precipitates should form by nucleation and growth during the cooling-down stage of the thermal annealing process at 1573 K. Magnesium in metallic form or other crystalline compound phases are not found. It should be pointed out that the two spots (red arrows) assumed to be from MgC_2 could originate from the double diffraction of Mg_2Si (001) that is forbidden for a perfect crystal.

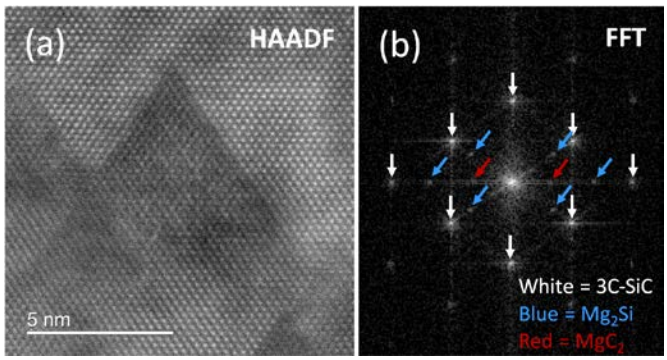

Figure 2. (a) High-resolution HAADF micrograph of 3C-SiC implanted to 9.6×10^{16} $^{25}Mg/cm^2$ at 673 K and annealed at 1573 K for 12 h in Ar. (b) FFT of (a).

Figure 3(a) shows a HAADF STEM micrograph near the damage peak in 3C-SiC. A region of ~25 nm × 25 nm that contained some dark and grey tetrahedra was selected for elemental mapping using EELS. The EELS maps are shown in Figures 3(b)-(d) for C, Si and Mg, respectively. A composite image for C, Si and Mg is shown in Figure 3(e). Clearly, there is Mg enrichment with concurrent depletion of Si and C in the dark tetrahedra, indicating that the Mg-bearing precipitates are formed inside the tetrahedra. However, the greyer tetrahedra in Figure 3(a) do not show a significant Mg concentration. They could be cavities or SFTs, but the exact nature of the tetrahedra still needs further studies. An intensity scan across two overlapping tetrahedra shown in Figure 3(e) was conducted and one-dimensional concentration profiles of Si, C and Mg are plotted in Figure 3(f). The percentages of the 3 elements are normalized to 100%. While the Si concentration shows a broad valley within the tetrahedra, it is interesting to notice that C concentration shows a small peak near the center of the precipitate, which is located at the minimum intensity of the double Mg peak profile. The overall higher concentrations of Si and C may be attributed to the predominant composition in the volume of the EELS analysis due to the

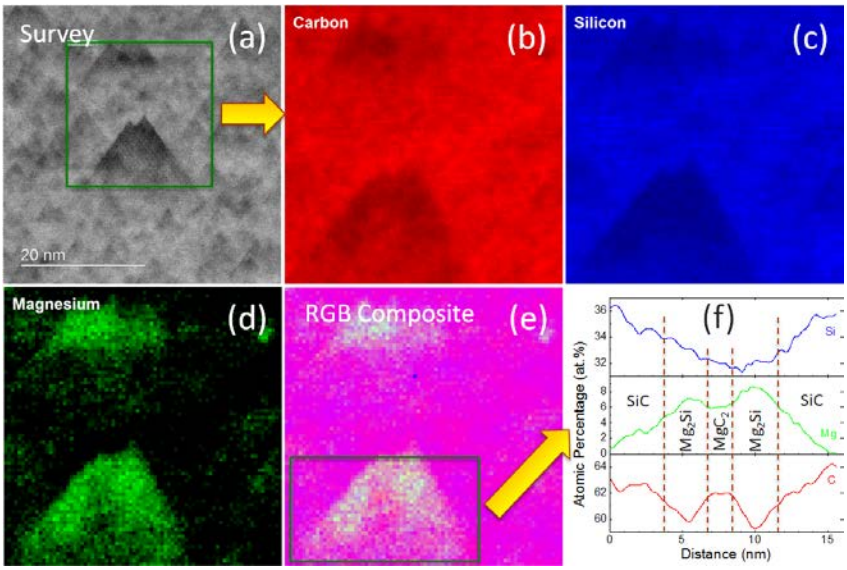

Figure 3. (a) HAADF micrograph of 3C-SiC implanted to 9.6×10^{16} $^{25}Mg/cm^2$ at 673 K and annealed at 1573 K for 12 h in Ar. EELS maps of (b) carbon, (c) silicon, (d) magnesium, and (e) all the elements. (f) Elemental profiles across a tetrahedron. Maps have been denoised using principal component analysis (PCA).

film thickness. From Figure 3(f), the Mg-bearing precipitate appears to have a core-shell structure, containing compositions of SiC, Mg_2Si, MgC_2, Mg_2Si, and SiC across the precipitate volume. The data may suggest formation of possible phases of Mg_2Si and MgC_2 in proximity, which would be reasonable. The lower Mg concentration in the Mg profile would be also understandable because the Mg concentration in MgC_2 is smaller than in Mg_2Si. It should be noted that such a core-shell structure is not always the case for all Mg-containing tetrahedra. Some tetrahedra show simply a single Mg peak overlapped with Si and C valleys without fine structures. Formation of the tetrahedral shape of the Mg-bearing precipitates is not yet well understood at this time. It could be associated with vacancy agglomeration on 3C-SiC {111} planes, facilitating formation of tetrahedral voids, while Mg atoms diffuses into the volume during annealing at 1573 K. As mentioned above, the vacancy concentration is expected to be significantly higher than the Mg concentration prior to annealing. Alternatively, there might be energetically favored interfaces containing Mg and Si or C. A model calculation should help understand the mechanism for the formation of the tetrahedral precipitates.

A series of iso-concentration surfaces at 10 at.% ^{25}Mg in 3C-SiC are shown in Figure 4 as a function of annealing temperature and duration. The two-dimensional plots are generated from a 10 nm slice of material in the Mg peak region. It is seen that the degree of homogeneity of the green dots that represent Mg clusters decreases with either increasing annealing temperature or duration. This indicates that Mg atoms tend to cluster more rapidly as temperature increases during isochronal annealing for 12 h; longer duration of annealing leads to growth of larger Mg clusters on the average at 1573 K. For 1573 K and 12 h annealed 3C-SiC, the number density of the Mg-bearing precipitates is estimated to be 1.6×10^{18} cm^{-3}, which is consistent with the STEM observation shown in Figure 1. The average size (discussed below) and the number density of the precipitates should increase and decrease, respectively, with the increase of either annealing temperature or duration. It should be mentioned that the shape of the Mg-bearing precipitates are not tetrahedra that were observed from STEM. This is mainly because there is a large field evaporation difference between Mg (~21 V/nm) and SiC (>33 V/nm). Under a fixed condition, Mg evaporates at a faster rate than Si and C, leading to shape deformation of the Mg-bearing precipitates during three-dimensional atom map reconstruction. In fact, different shapes of Mg-bearing precipitates

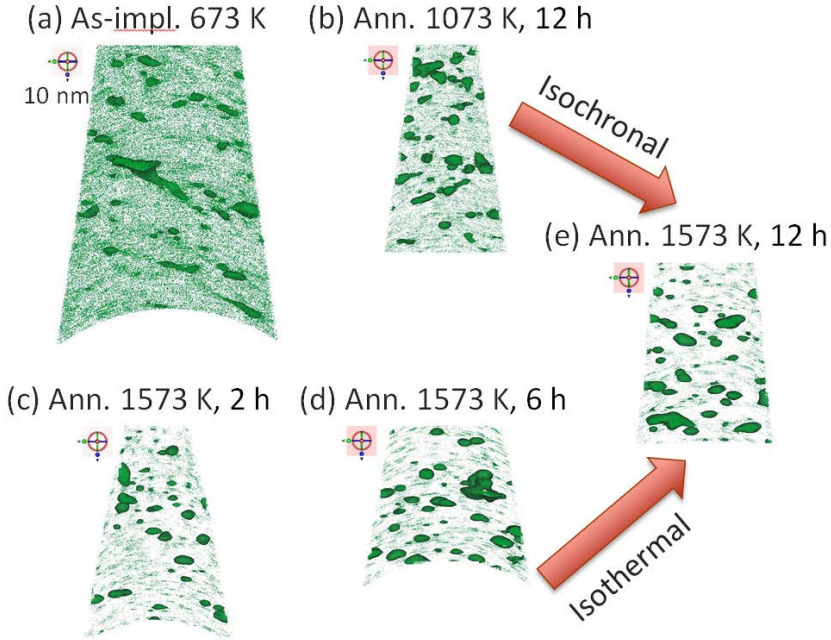

Figure 4. Iso-concentration surface at 10 at.% ^{25}Mg in 3C-SiC (a) implanted to 9.6×10^{16} ^{25}Mg/cm^2 at 673 K, and annealed at (b) 1073 K, 12 h, (c) 1573 K, 2 h, (d) 1573 K, 6 h, and (e) 1573 K, 12 h in Ar.

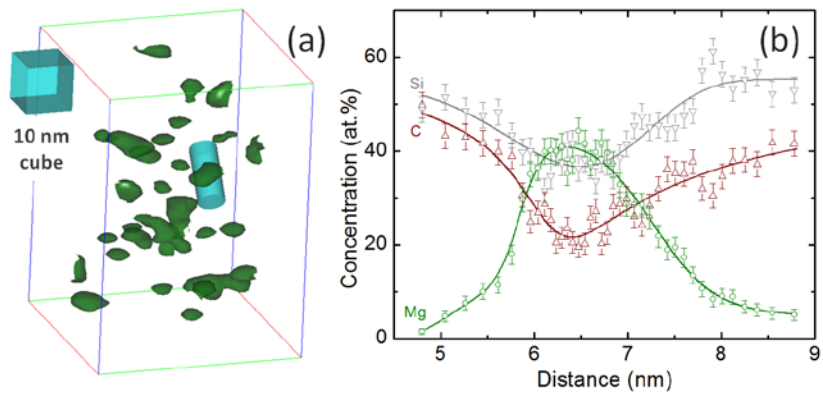

Figure 5. (a) Iso-concentration surface of ^{25}Mg at 16 at.% in 3C-SiC implanted to 9.6×10^{16} ^{25}Mg/cm^2 at 673 K and annealed at 1573 K for 12 h in Ar. (b) Concentration profiles of Si, C and Mg of the cluster scanned through a cylinder shown in (a).

are observed, including three-dimensional cluster shaped, plate-like, and curvilinear features through a series of cross sectional views of iso-concentration surfaces (data not shown).

A three-dimensional image of Mg-bearing clusters at surface concentration of 16 at.% ^{25}Mg in the implanted 3C-SiC annealed at 1573 K for 12 is shown in Figure 5(a). At this surface concentration, Mg-bearing clusters have sizes ranging from a few to over 10 nm. One-dimensional concentration profiles of Si, C and Mg from a cylinder scan across a selected precipitate indicated in Figure 5(a) are shown in Figure 5(b). The data show a distinct Mg concentration peak with a maximum of over 40 at.% Mg overlapped with depletion of both Si and C in the volume. The result is generally consistent with the EELS data (not shown) for this sample. There are also some precipitates that have the maximum concentration in excess of 80 at.% Mg [3], but diffraction spots of pure Mg metal are not observed from this sample.

An iso-concentration surface at 2.7 at.% ^{25}Mg is used in this study to define Mg precipitates for size analysis. In general, a lower surface concentration leads to a larger precipitate size because small clusters can be artificially connected into larger ones at low surface concentrations. For comparison, two definitions are used to calculate the precipitate size distribution. The first one is based on the radius of gyration R_g, which is the radius of a hypothetical body having all its mass concentration at a single distance from its center of mass, while having the same mass and the moment of inertia as the object [9]. For three dimensional precipitates, the hypothetical body is a spherical shell with a radius:

$$R_g = \sqrt{\left(R_{gx}^2 + R_{gy}^2 + R_{gz}^2\right)/3}, \qquad (1)$$

where R_{gx}, R_{gy} and R_{gz} represent the radii of gyration in x, y and z directions. This value could underestimate the precipitate size [9] and is considered as the lower bound of the precipitates. The upper bound that could overestimate the precipitate size is defined as the extent dimension that accounts for the furthest Mg ions in the precipitates:

$$R_e = \sqrt{\left(R_{ex}^2 + R_{ey}^2 + R_{ez}^2\right)/3}. \qquad (2)$$

Figure 6(a) shows the distributions of the total ranged Mg ions with the maximum R_g and R_e values equal to 7.7 and 19.3 nm, respectively. From the data, the mean radius is estimated to be from 0.9 to 2.2 nm, or precipitate size (diameter) from 1.8 to 4.4 nm. The second definition used in this study for estimation of the size is based on the precipitate volumes V_{Rg} and V_{Re}, representing the lower and upper bounds, respectively. The results from the analysis are plotted in Figure 6(b) with the maximum volumes V_{Rg} and

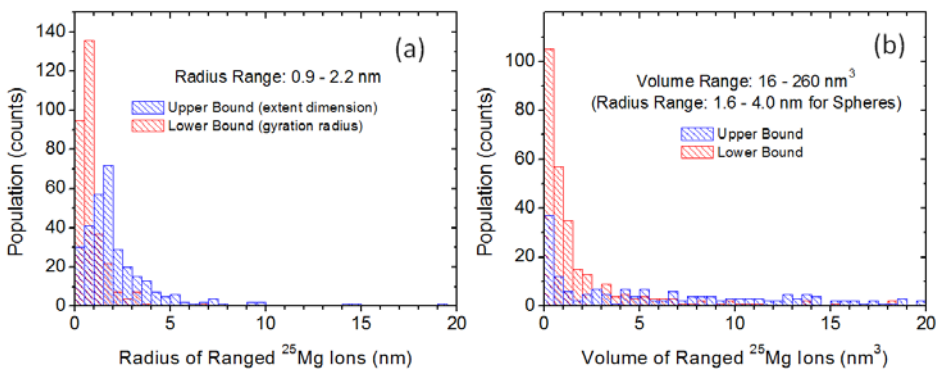

Figure 6. Size distribution as a function of (a) radius and (b) volume of ^{25}Mg-bearing precipitates, defined by iso-concentration surface at 2.7 at.% ^{25}Mg in 3C-SiC implanted to 9.6×10^{16} ^{25}Mg/cm^2 at 673 K and annealed at 1573 K for 12 h in Ar.

V_{Re} equal to 1,622 and 26,155 nm^3 that are out of the display range in the figure. The mean volumes of the precipitates are between 16 and 260 nm^3, equivalent to mean radii of 1.6 to 4.0 nm for a spherical shape. The corresponding size of the precipitates ranges from 3.2 to 8 nm, which is consistent with the STEM observation of 2-8 nm (Figure 1).

Acknowledgements

This research was supported by Office of Fusion Energy Sciences, U.S. Department of Energy (DOE) under Contract DE-AC05-76RL01830. Ion implantation was performed at the Ion Beam Materials Laboratory through partial support from the Center for Integrated Nanotechnologies (CINT), a DOE nanoscience user facility jointly operated by Los Alamos and Sandia National Laboratories. TEM and APT were performed under a general user proposal at the Environmental Molecular Sciences Laboratory (EMSL), a national scientific user facility located at PNNL. Isotope ^{25}Mg used in this research was supplied by the DOE Office of Science Isotope Program in the Office of Nuclear Physics.

References

[1] M. E. Sawan, Y. Katoh, and L. L. Snead, J. Nucl. Mater. 442 (2013) S370.
[2] W. Jiang, H. J. Jung, L. Kovarik, Z. Wang, T. J. Roosendaal, Z. Zhu, D. J. Edwards, S. Y. Hu, C. H. Henager, Jr., R. J. Kurtz, and Y. Wang, J. Nucl. Mater. 458 (2015) 146.
[3] W. Jiang, J. Liu, D. K. Schreiber, D. J. Edwards, C. H. Henager, Jr., R. J. Kurtz, and Y. Wang, Fusion Materials Semiannual Progress Report for Period Ending December 31, 2015, DOE/ER-0313/59, U.S. Department of Energy, 79.
[4] W. Jiang, J. Zhang, Z. Zhu, T. J. Roosendaal, S. Y. Hu, C. H. Henager, Jr., R. J. Kurtz, and Y. Wang, Fusion Materials Semiannual Progress Report for Period Ending June 30, 2015, DOE/ER-0313/58, U.S. Department of Energy, 119.
[5] J. F. Ziegler, J. P. Biearsack, and U. Littmark, *The stopping and Range of Ions in Solids* (Pergamon Press, New York, 1985); available from: http://www.SRIM.org/.
[6] S. Kondo, Y. Katoh, and L. L. Snead, Appl. Phys. Lett. 93 (2008) 163110.
[7] Y. N. Osetsky, D. Rodney, and D. J. Bacon, Phil. Mag. 86 (2006) 2295.
[8] R. A. Coward, C. R. Winkler, W. A. Hanson, M. L. jablonski, and M. L. Taheri, J. Nucl. Mater. 457 (2015) 298.
[9] M. K. Miller and R. G. Forbes, Atom-Probe Tomography: *The Local Electrode Atom Probe* (Srpinger, New York, 2014), p.319.